EUROPEAN JOURNAL OF COMPUTATIONAL MECHANICS
2018, VOL. 27, NOS. 5–6, 443–468
https://doi.org/10.1080/17797179.2018.1550379

Taylor & Francis
Taylor & Francis Group

Axisymmetric MHD viscous flows bounded by a solid plane normal to a uniform ambient magnetic field: fundamental flows and application to a solid sphere translating normal to the wall

A. Sellier[a] and S. H. Aydin[b]

[a]LadHyX. Ecole Polytechnique, Palaiseau Cédex, France; [b]Department of Mathematics, Karadeniz Technical University, Trabzon, Turkey

ABSTRACT

This work first determines two axisymmetric fundamental Magneto Hydrodynamic (MHD) flows induced, in a conducting Newtonian liquid domain bounded by a plane wall, by distributing either radial or axial points forces on a circular ring located in a plane parallel with the wall and normal to a prescribed uniform ambient magnetic field $\mathbf{B} = B\mathbf{e}_z$. This is achieved, for both a perfectly conducting and an insulating wall, by using the fundamental flow due to a source point analytically obtained elsewhere. Each resulting axisymmetric fundamental MHD flow velocity components (radial and axial ones) and pressure is then analytically expressed in terms of one-dimensional integrals and of the so-called Hartmann layer thickness $d = (\sqrt{\mu/\sigma})/|B|$. These quantities are numerically calculated and the wall–ring interactions are then discussed. Such interactions are found to deeply affect the fundamental flows' streamlines and pressure field prevailing in an unbounded liquid. The derived fundamental flows are then employed to investigate, using a boundary formulation, the drag experienced by a solid sphere immersed in the liquid and translating normal to the wall.

ARTICLE HISTORY
Received 30 November 2017
Accepted 24 September 2018

KEYWORDS
Magneto hydrodynamics; axisymmetric fundamental flow; circular shape source; bounded flow; plane wall; sphere

1. Introduction

It is of importance for many applications to get the flow about a solid particle experiencing a prescribed rigid-body migration in a conducting Newtonian liquid with uniform density ρ_l, viscosity μ and conductivity $\sigma > 0$. Far from the body, the liquid is quiescent and subject to a prescribed uniform magnetic field $\mathbf{B} = B\mathbf{e}_z$ and no electric field. In the liquid, the flow, with velocity $\mathbf{u}$ and pressure p, experiences the Lorentz body force $\mathbf{f}_L = \mathbf{j} \wedge \mathbf{B}'$ with $\mathbf{B}'$ the magnetic field and $\mathbf{j}$ the current density. For most applications, this latter vector obeys the Ohm's law $\mathbf{j} = \sigma(-\nabla\phi + \mathbf{u} \wedge \mathbf{B}')$,

CONTACT A. Sellier sellier@ladhyx.polytechnique.fr

with ϕ the electric potential and $\mathbf{E} = -\nabla\phi$ the associated electric field. Accordingly, the flow $(\mathbf{u}, p)$ is coupled (through the Lorentz body force) with $(\phi, \mathbf{B}')$ and the determination of $(\mathbf{u}, p, \phi, \mathbf{B}')$ falls in the scope of the so-called Magneto Hydrodynamics (Branover & Tsinober, 1970; Moreau, 1990; Tsinober, 1970). In the absence of additional assumptions, getting $(\mathbf{u}, p, \phi, \mathbf{B}')$ is, even for a spherical body, a very involved task because these quantities are governed by the coupled Maxwell and non-linear Navier-Stokes equations. For a velocity with a typical magnitude V, a body with length scale a and a liquid with a uniform magnetic permeability $\mu_m > 0$, the quantities $(\mathbf{u}, p, \phi, \mathbf{B}')$ depend upon the body shape and motion, but also upon three dimensionless numbers: the magnetic Reynolds number $\mathrm{Re}_m = \mu_m \sigma |V| a$, the Reynolds number $\mathrm{Re} = \rho_l V a / \mu$, and the Hartmann number $\mathrm{Ha} = a/d$, where the length $d = (\sqrt{\mu/\sigma})/|B|$ is the so-called Hartmann layer thickness (Hartmann, 1937).

Assuming $\mathrm{Re}_m \ll 1$ and a body to admit the same uniform magnetic permeability μ_m as the liquid yields $\mathbf{B}' = \mathbf{B}$ (Tsinober, 1970). For a solid asymmetric body translating parallel to both its axis of revolution and the magnetic field, then $\mathbf{E} = \mathbf{0}$! (see, for instance, Gotoh, 1960) and one thus ends up with only two unknown termed as the Magneto Hydrodynamic (MHD) fields, namely $\mathbf{u}$ and p. The MHD flow $(\mathbf{u}, p)$ depends upon $(\mathrm{Ha}, \mathrm{Re})$ and its determination for arbitrary translating axisymmetric bodies is still a cumbersome task. For a spherical body translating parallel to the ambient magnetic field $\mathbf{B}$, the solution was asymptotically obtained by Chester (1957) for $\mathrm{Ha} \ll 1$ and by Chester (1961) for $\mathrm{Ha} \gg 1$ under the assumption of negligible inertia effects, i.e. for $\mathrm{Re} \ll 1$. In such circumstances, the MHD flow $(\mathbf{u}, p)$ is termed as creeping or viscous flow. Recently, Sellier & Aydin (2016) proposed a new boundary method to treat, in the entire range $\mathrm{Ha} > 0$, the case of the translating sphere addressed by Chester (1957; 1961). The procedure appeals to the axisymmetric fundamental MHD viscous flows obtained by Sellier & Aydin (2016) and produced by putting a radial or axial distribution of source points on a circular ring. This was actually made possible by using the coupled fundamental MHD flow and electric potential, analytically determined by Priede (2013), induced by a point force.

All of aforementioned papers consider the case of an unbounded liquid domain. However, bounded liquid domains are also encountered in applications. This strongly suggests extending (Sellier & Aydin, 2017) to the case of a sphere translating still parallel with the ambient uniform magnetic field $\mathbf{B}$, but in a conducting liquid bounded by a plane wall parallel to $\mathbf{B}$. Following Sellier & Aydin (2017), it is then necessary to determine the axisymmetric fundamental flows produced by spreading a radial or axial distribution of source points on a circular ring located in a plane parallel to

the bounding wall (i.e. to extend (Sellier & Aydin, 2017) to the bounded liquid case). This key issue is the object of the present work together with its application to the determination of the drag experienced by a solid sphere translating normal to the wall.

The paper is organised as follows. The governing MHD equations for the coupled electric potential and flow about a solid body moving in a conducting liquid near a solid plane wall, together with the relevant fundamental axisymmetric MHD flows in the case of a problem of revolution, are presented in Section 2. These bounded fundamental flows, obtained by putting on a circular ring a radial of axial force distribution, are determined in Section 3 by appealing to the bounded fundamental flow (and electrical potential) produced by a point force recently obtained analytically by Sellier (2017). The numerical implementation is handled in Section 4, together with the discussion of a few computed unbounded and bounded fundamental flows patterns. Using the determined fundamental flows, the drag experienced by a solid sphere translating normal to the wall is then investigated in Section 5. Finally, concluding remarks are given in Section 6.

2. Motivating problem. Relevant bounded axisymmetric fundamental MHD flows

This section presents a motivating axisymmetric problem and the two associated fundamental and bounded axisymmetric MHD flows to be determined in the present work.

2.1. Motivating bounded MHD problem

For applications, it is required to get the flow about a solid particle experiencing a given rigid-body velocity field $\mathbf{u}_{rb}$ in a conducting Newtonian liquid subject to a uniform ambient magnetic field $\mathbf{B} = B\mathbf{e}_z$ and bounded by a motionless and no-slip $z = 0$ plane wall Σ. This problem is illustrated in Figure 1 for a solid sphere translating near and normal to the $z = 0$ wall with velocity $U\mathbf{e}_z$.

As mentioned in Introduction, the liquid flow, with velocity $\mathbf{u}$ and pressure p, is in general coupled to a non-uniform electric potential ϕ and the magnetic field $\mathbf{B}'$ prevailing in the liquid. The flow $(\mathbf{u}, p)$ is subject to the Lorentz body force $\mathbf{f}_L = \mathbf{j} \wedge \mathbf{B}'$, with $\mathbf{j}$ the current density. Moreover, $\mathbf{j}$ obeys the widely employed Ohm's law $\mathbf{j} = \sigma(\mathbf{u} \wedge \mathbf{B}' - \nabla\phi)$, where $\sigma > 0$ denotes the fluid uniform conductivity. In summary, the problem consists of obtaining in the entire liquid domain the coupled MHD fields, namely the flow $(\mathbf{u}, p)$, the magnetic field $\mathbf{B}'$ and the electric field $\mathbf{E} = -\nabla\phi$. In general, such a task is tremendously involved since one has to simultaneously solve

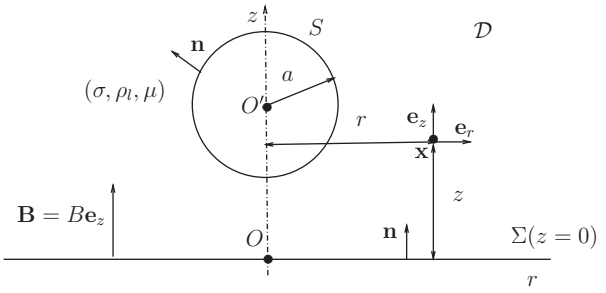

Figure 1. A solid sphere translating normal to the $z = 0$ plane wall Σ in a conducting Newtonian liquid.

coupled and unsteady non-linear Navier-Stokes equations and Maxwell equations. Of course, the required MHD solution $(\mathbf{u}, p, \mathbf{B}', \phi)$ depends upon the body shape, location and rigid-body motion $\mathbf{u}_{rb}$.

Fortunately, adding a few assumptions to the problem Reynolds number Re and magnetic Reynolds number Re_m makes it possible to face a more tractable issue. These numbers are based on the velocity $\mathbf{u}$ typical magnitude $V > 0$, the solid length scale a and also the Newtonian liquid uniform density ρ_l, viscosity μ and magnetic permeability μ_m. More precisely, $\mathrm{Re} = \rho_l V a/\mu$ and $\mathrm{Re}_m = \mu_m \sigma V a$. First, all inertial effects are neglected, i.e. $\mathrm{Re} \ll 1$, and one speaks of viscous or creeping flow $(\mathbf{u}, p)$. Since for most applications $\mathrm{Re}_m \ll \mathrm{Re}$, note that $\mathrm{Re}_m \ll 1$. This latter property, together with the assumption of a body having the same uniform magnetic permeability μ_m as the liquid, shows that the ambient imposed magnetic field $\mathbf{B}$ is not affected by the flow $(\mathbf{u}, p)$ and the electric field $\mathbf{E}$. Accordingly, $\mathbf{B}' = B\mathbf{e}_z$ in the entire bounded liquid domain $\mathcal{D}$. Assuming a quasi-steady flow and requiring the charge conservation $\nabla.\mathbf{j} = 0$ in the liquid finally yields for $(\mathbf{u}, p, \phi)$ the coupled equations

$$\mu \nabla^2 \mathbf{u} = \nabla p + \sigma B \nabla \phi \wedge \mathbf{e}_z - \sigma B^2 (\mathbf{u} \wedge \mathbf{e}_z) \wedge \mathbf{e}_z \text{ and } \nabla.\mathbf{u} = 0 \text{ in } \mathcal{D}, \tag{1}$$

$$\Delta \phi = B \nabla.(\mathbf{u} \wedge \mathbf{e}_z) \text{ in } \mathcal{D}. \tag{2}$$

Equations (1) and (2) must be supplemented with relevant far-field behaviours and boundary conditions on $S \cup \Sigma$ for $(\mathbf{u}, p, \phi)$. Henceforth, we shall use Cartesian coordinates (O, x, y, z), with the origin O on the wall Σ and associated unit vectors $(\mathbf{e}_x, \mathbf{e}_y, \mathbf{e}_z)$. Hence (see also Figure 1), $\mathbf{x} = \mathbf{OM} = x\mathbf{e}_x + y\mathbf{e}_y + z\mathbf{e}_z$ for an arbitrary point M. The origin O is taken so that $(x^2 + y^2)^{1/2} = O(a)$ for any point M located on the body surface S. Assuming a no-slip boundary S, a no-slip motionless wall Σ and a flow quiescent far from the body, it is required that

$$(\mathbf{u}, p) \to (\mathbf{0}, 0) \text{ as } |\mathbf{x}| \to \infty, \quad \mathbf{u} = \mathbf{u}_{rb} \text{ on } S, \quad \mathbf{u} = \mathbf{0} \text{ on } \Sigma, \tag{3}$$

where it is recalled that $\mathbf{u}_{rb}$ designates the prescribed rigid-body velocity. There is no electric field far from the body. In addition, the surface S, with the unit normal vector $\mathbf{n}$ pointing into the liquid, is insulating so that the condition $\mathbf{j}.\mathbf{n} = 0$ is required there (Moreau, 1990). Finally, the wall with unit surface vector $\mathbf{n} = \mathbf{e}_z$, is either perfectly conducting (condition $\mathbf{j} \wedge \mathbf{n} = 0$ as shown by Moreau, 1990; Tsinober, 1970) or insulating (condition $\mathbf{j}.\mathbf{e}_z = 0$). Taking into account both the Ohm's law $\mathbf{j} = \sigma(\mathbf{u} \wedge \mathbf{B} - \nabla\phi)$ and the velocity boundary conditions (Equation (3)) on Σ, yields the following conditions:

$$\nabla\phi \to \mathbf{0} \text{ as} |\mathbf{x}| \to \infty, \quad \nabla\phi.\mathbf{n} = B(\mathbf{u}_{rb} \wedge \mathbf{e}_z).\mathbf{n} \text{ on } S, \tag{4}$$

$$\phi = 0 \text{ (conducting) or } \nabla\phi.\mathbf{e}_z = 0 \text{ (insulating) on } \Sigma(z = 0). \tag{5}$$

As mentioned in Introduction, the solution $(\mathbf{u}, p, \phi)$ to Equations (1)–(5) depends upon the Hartmann number $\mathrm{Ha} = a/d$, where $d = \sqrt{\mu/\sigma}/|B|$ is the so-called Hartmann layer thickness (Hartmann, 1937). Even for the two previous types of walls (conducting or insulating) it remains very difficult to gain $(\mathbf{u}, p, \phi)$ for arbitrary Ha, body shape and rigid-body motion because $\mathbf{u}$ and ϕ are coupled through Equation (2) and boundary condition.

2.2. Axisymmetric case. Relevant bounded axisymmetric fundamental MHD viscous flows

Considering, as illustrated for a sphere in Figure 1, a solid body of revolution about the $(O, \mathbf{e}_z)$ axis translating normal to the wall at the velocity $U\mathbf{e}_z$ results in a much more tractable MHD problem! In such circumstances, the cylindrical polar coordinates (r, θ, z) are employed, with $r = \{x^2 + y^2\}^{1/2} \geq 0, \theta \in [0, 2\pi]$, and also $x = r\cos\theta, y = r\sin\theta$. The associated local unit vectors, also shown in Figure 1, are $\mathbf{e}_r(\theta) = \cos\theta\mathbf{e}_x + \sin\theta\mathbf{e}_y$ and $\mathbf{e}_\theta(\theta) = \mathbf{e}_z \wedge \mathbf{e}_r$. Note that Equation (4) yields $\nabla\phi.\mathbf{n} = 0$ on S. Thus, boundary conditions (Equations 3–5) on $S \cup \Sigma$ become axisymmetric ones. Accordingly, the flow $(\mathbf{u}, p)$ is axisymmetric *without swirl*, i.e. it reads as $\mathbf{u}(\mathbf{x}) = u_r(r, z)\mathbf{e}_r + u_z(r, z)\mathbf{e}_z$ and $p(\mathbf{x}) = p(r, z)$ at point $M(r, \theta, z)$ in the liquid domain. Consequently, $\nabla.(\mathbf{u} \wedge \mathbf{e}_z) = 0$ and ϕ obeys the well-posed problem

$$\Delta\phi = 0 \text{ in } \mathcal{D}, \nabla\phi \to \mathbf{0} \text{ as} |\mathbf{x}| \to \infty, \nabla\phi.\mathbf{n} = 0 \text{ on } S, \tag{6}$$

$$\phi = 0 \text{ (conducting) or } \nabla\phi.\mathbf{e}_z = 0 \text{ (insulating) on } \Sigma(z = 0). \tag{7}$$

In the entire fluid domain $\mathcal{D}$, the solution to Equations (6) and (7) is given by $\phi = 0$ or $\nabla\phi = \mathbf{0}$ for the conducting or insulating wall case, respectively. Thus, for the axisymmetric MHD problem, there is no electric field.

For symmetry reasons, the axisymmetric flow $(\mathbf{u}, p)$ with stress tensor σ exerts on the body boundary S a surface traction $\mathbf{f} = \sigma.\mathbf{n}$ taking the form $\mathbf{f} = f_r(r,z)\mathbf{e}_r + f_z(r,z)\mathbf{e}_z$. Therefore, the flow $(\mathbf{u}, p)$ is obtained by superposing the axisymmetric flows defined in the $z>0$ domain, having zero velocity on the $z = 0$ wall and produced by distributing on a circular ring located on S axisymmetric point forces. Denoting by δ the usual Dirac pseudo-function, we then consider the fundamental flow produced by the axisymmetric body force $F\delta(r - r_0)\delta(z - z_0)\mathbf{s}$ distribution, with non-zero force strength F and local unit vector $\mathbf{s}$, spread on the circular ring with radius r_0 and location $z_0>0$. This axisymmetric flow velocity $u_\mathbf{s}(\mathbf{x})$ and pressure $p_\mathbf{s}(\mathbf{x})$ satisfy

$$\begin{aligned} &\mu\nabla^2\mathbf{u}_\mathbf{s} = \nabla p_\mathbf{s} - \sigma B^2(\mathbf{u}_\mathbf{s} \wedge \mathbf{e}_z) \wedge \mathbf{e}_z - F\delta(r - r_0)\delta(z - z_0)\mathbf{s} \; for \; z > 0, \\ &\nabla.\mathbf{u}_\mathbf{s} = 0 \text{ for } z>0, \end{aligned} \tag{8}$$

$$(\mathbf{u}_\mathbf{s}, p_\mathbf{s}) \to (\mathbf{0}, 0) \text{ as } \sqrt{(r - r_0)^2 + (z - z_0)^2} \to \infty, \quad \mathbf{u}_\mathbf{s} = \mathbf{0} \text{ on } \Sigma. \tag{9}$$

By superposition, we shall consider two so-called fundamental flows produced by putting at each point $M_0(r_0, z_0, \theta_0)$ of the circular ring an axial force (case $\mathbf{s} = \mathbf{e}_z$) or a radial force (case $\mathbf{s} = \mathbf{e}_r$.) These flows are determined in the next section.

3. Adopted procedure and resulting fundamental flows

This section obtains analytically the required axisymmetric fundamental flows from the knowledge of the fundamental and coupled MHD flow and electric potential induced in the bounded $z>0$ liquid domain by a concentrated unit force, of strength $F\mathbf{e}_z$ or $F\mathbf{e}_x$, placed at one point $\mathbf{x}_0$ in the liquid.

3.1. Fundamental bounded coupled MHD flow and electric potential

From Section 2.2, we build the axisymmetric fundamental flow $(\mathbf{u}_\mathbf{s}, p_\mathbf{s})$ by superposing the fundamental flows produced by a concentrated force, with strength $F\mathbf{s}$, located at a given arbitrary point $\mathbf{x}_0$ of the circular ring with given radius r_0 and location $z_0>0$. The fundamental flow produced by a concentrated point force with strength $\mathbf{g}$ located at a given point $\mathbf{x}_0$ has velocity $\mathbf{v}$ and pressure q. Except for $\mathbf{g}$ parallel to the magnetic field $\mathbf{B} = B\mathbf{e}_z$, this flow is not asymmetric about the $(O, \mathbf{e}_z)$ axis and it is coupled to

an electric potential ψ. For the conducting or insulating wall Σ the MHD quantities $(\mathbf{v}, q, \psi)$ then obey (recall Section 2.1)

$$\mu\nabla^2\mathbf{v} = \nabla q + \sigma B\nabla\boldsymbol{\phi} \wedge \mathbf{e}_z - \sigma B^2(\mathbf{v} \wedge \mathbf{e}_z) \wedge \mathbf{e}_z - \delta(\mathbf{x} - \mathbf{x}_0)\mathbf{g} \text{ for } z > 0, \tag{10}$$

$$\nabla.\mathbf{v} = 0 \text{ and } \Delta\psi = B\nabla.(\mathbf{v} \wedge \mathbf{e}_z) \text{ for } z > 0, \tag{11}$$

$$(\mathbf{v}, q, \nabla\boldsymbol{\phi}) \to (\mathbf{0}, 0, \mathbf{0}) \text{ as} |\mathbf{x} - \mathbf{x}_0| \to \infty \text{ and } \mathbf{v} = \mathbf{0} \text{ on } \Sigma, \tag{12}$$

$$\psi = 0 \,(\text{conducting}) \text{ or } \nabla\psi.\mathbf{e}_z = 0 (\text{insulating}) \text{ on } \Sigma(z = 0). \tag{13}$$

The above MHD problem (Equations 10–13) is linear in $\mathbf{g}$. Consequently, one can introduce the so-called second-rank Green velocity tensor $\mathbf{V}(\mathbf{x}, \mathbf{x}_0)$, pressure vector $\mathbf{Q}(\mathbf{x}, \mathbf{x}_0)$ and potential vector $\boldsymbol{\Phi}(\mathbf{x}, \mathbf{x}_0)$, such that

$$\mu\mathbf{v}(\mathbf{x}) = \mathbf{V}(\mathbf{x}, \mathbf{x}_0).\mathbf{g}, \quad q(\mathbf{x}) = \mathbf{Q}(\mathbf{x}, \mathbf{x}_0).\mathbf{g}, \quad \Psi(\mathbf{x}) = \boldsymbol{\Phi}(\mathbf{x}, \mathbf{x}_0).\mathbf{g}. \tag{14}$$

The Cartesian components $V_{lt} = \mathbf{e}_l.\mathbf{v}.\mathbf{e}_t, Q_t = \mathbf{Q}.\mathbf{e}_t$ and $\Phi_t = \boldsymbol{\Phi}.\mathbf{e}_t$ have been recently derived *analytically* by Sellier (2017) by performing a two-dimensional Fourier transform on variables x and y, for $t = x, z$ and $l = x, y, z$. These components, available in the work by Sellier (2017) and not reproduced here, have been found to solely depend upon $(x - x_0, y - y_0, z, z_0; d)$, where it is recalled that length $d = \sqrt{\mu/\sigma}/|B|$ is the Hartmann layer thickness and (x, y, z) and (x_0, y_0, z_0) are the Cartesian coordinates of points $\mathbf{x}$ and $\mathbf{x}_0$, respectively.

3.2. Derivation of the fundamental axisymmetric MHD flows

The required axisymmetric fundamental flow $(\mathbf{u}_\mathbf{s}, p_\mathbf{s})$ governed by Equations (8) and (9) is built using the previous relations (Equation (14)). Dropping henceforth the dependence in $\boldsymbol{s}$, its axisymmetric velocity field $\mathbf{u}$ and pressure field p read, at point $\mathbf{x}$ with cylindrical coordinates (r, z, θ),

$$\mathbf{u}(\mathbf{x}) = u_r(r, z)\mathbf{e}_r + u_z(r, z)\mathbf{e}_z, \quad p(\mathbf{x}) = p(r, z). \tag{15}$$

The quantities $u_r(r, z), u_z(r, z)$ and $p(r, z)$ are here obtained by taking $\theta = 0$ and, therefore, $x = r$ and $y = 0$, while the points $\mathbf{x}_0$ on the circular ring have the polar coordinates (r_0, z_0, θ_0), with $\theta \in [0, 2\pi]$ and $x_0 = r_0 \cos\theta_0, y_0 = r_0 \sin\theta_0$. The following cases are considered:

Case 1: The fundamental flow due to the axial force distribution (choice $\mathbf{s} = \mathbf{e}_z$). As shown by Sellier (2017), $\Phi_z = 0$ and thus there is no electric field associated with the fundamental flow $(\mathbf{u}, p)$ in that case. Moreover, one readily arrives at the solution

$$\mu u_r(r,z) = F\int_0^{2\pi} V_{xz}(r - r_0\cos\theta_0, -r_0\sin\theta_0, z, z_0; d)d\theta_0, \tag{16}$$

$$\mu u_z(r,z) = F\int_0^{2\pi} V_{zz}(r - r_0\cos\theta_0, -r_0\sin\theta_0, z, z_0; d)d\theta_0, \tag{17}$$

$$p(r,z) = F\int_0^{2\pi} Q_z(r - r_0\cos\theta_0, -r_0\sin\theta_0, z, z_0; d)d\theta_0. \tag{18}$$

Case 2: The fundamental flow due to the radial force distribution (choice $\mathbf{s} = \mathbf{e}_r(\theta_0)$). Since $\mathbf{e}_r(\theta_0) = \cos\theta_0\mathbf{e}_x + \sin\theta_0\mathbf{e}_y$, it follows that

$$\mu u_r(r,z) = F\int_0^{2\pi} \{\cos\theta_0 V_{xx}(r - r_0\cos\theta_0, -r_0\sin\theta_0, z, z_0; d) + \sin\theta_0 V_{xy}(r - r_0\cos\theta_0, -r_0\sin\theta_0, z, z_0; d)\}d\theta_0, \tag{19}$$

$$\mu u_z(r,z) = F\int_0^{2\pi} \{\cos\theta_0 V_{zx}(r - r_0\cos\theta_0, -r_0\sin\theta_0, z, z_0; d) + \sin\theta_0 V_{zy}(r - r_0\cos\theta_0, -r_0\sin\theta_0, z, z_0; d)\}d\theta_0. \tag{20}$$

Similarly, the associated pressure reads,

$$p(r,z) = F\int_0^{2\pi} \{\cos\theta_0 Q_x(r - r_0\cos\theta_0, -r_0\sin\theta_0, z, z_0; d) + \sin\theta_0 Q_y(r - r_0\cos\theta_0, -r_0\sin\theta_0, z, z_0; d)\}d\theta_0. \tag{21}$$

As shown at the end of Section 2.1, we expect the electrical potential Ψ to be constant in the liquid. At that stage, we however obtain by superposition Ψ as follows:

$$\psi(r,z) = F\int_0^{2\pi} \{\cos\theta_0 \Psi_x(r - r_0\cos\theta_0, -r_0\sin\theta_0, z, z_0; d) + \sin\theta_0 \Psi_y(r - r_0\cos\theta_0, -r_0\sin\theta_0, z, z_0; d)\}d\theta_0. \tag{22}$$

However, using the analytical form of Ψ_x given by Sellier (2017) and the one of Ψ_y (easily obtained by repeating the procedure detailed by Sellier (2017)) shows that, for symmetry reasons, the integral on the right-hand side of Equation (22) vanishes. It follows that, as expected, $\psi = 0$.

Identities (Equations 16–22) are analogous to the ones used by Sellier & Aydin (2016) for the *unbounded* flow case, i.e. in the absence of the wall Σ.

For convenience, we henceforth use for each above fundamental flow the decompositions

$$u_r = u_r^{\infty} + u_r^{w}, \quad u_z = u_z^{\infty} + u_z^{w}, \quad p = p^{\infty} + p^{w}, \tag{23}$$

with $(u_r^{\infty}, u_z^{\infty}, p^{\infty})$ the flow obtained for the unbounded case and $(u_r^{w}, u_z^{w}, p^{w})$ an additional flow due to the wall Σ.

3.3. Fundamental bounded flow produced by an axial force distribution

The solution $(u_r^{\infty}, u_z^{\infty}, p^{\infty})$ has been derived analytically by Sellier & Aydin (2016). For the distance R and the function g defined as

$$\begin{aligned} R &= |\mathbf{x} - \mathbf{x}_0| = \{r^2 + r_0^2 - 2rr_0\cos\theta_0 + (z - z_0)^2\}^{1/2}, \\ g(t,d) &= [\mathrm{e}^{-t/(2d)}]/t \end{aligned} \tag{24}$$

it is expressed as follows:

$$\left[\frac{8\pi\mu}{F}\right] u_r^{\infty}(r,z) = \sinh\left(\frac{z - z_0}{2d}\right) \int_0^{2\pi} \left[\frac{g(R,d)}{R}\right] \left[1 + \frac{2d}{R}\right] (r - r_0\cos\theta_0) d\theta_0, \tag{25}$$

$$\begin{aligned} \left[\frac{8\pi\mu}{F}\right] u_z^{\infty}(r,z) &= \cosh\left(\frac{z - z_0}{2d}\right) \int_0^{2\pi} g(R,d) d\theta_0 \\ &\quad + (z - z_0)\sinh\left(\frac{z - z_0}{2d}\right) \int_0^{2\pi} \left[\frac{g(R,d)}{R}\right] \left[1 + \frac{2d}{R}\right] d\theta_0, \end{aligned} \tag{26}$$

$$\begin{aligned} \left[\frac{8\pi d}{F}\right] p^{\infty}(r,z) &= \sinh\left(\frac{z - z_0}{2d}\right) \int_0^{2\pi} g(R,d) d\theta_0 \\ &\quad + (z - z_0)\cosh\left(\frac{z - z_0}{2d}\right) \int_0^{2\pi} \left[\frac{g(R,d)}{R}\right] \left[1 + \frac{2d}{R}\right] d\theta_0. \end{aligned} \tag{27}$$

Appealing to both Sellier (2017) and the above solution for the unbounded fluid, the identities (Equations 16–18) now provide the following relations:

$$\begin{aligned} \left[\frac{8\pi\mu}{F}\right] u_r^{w}(r,z) &= -\sinh\left(\frac{z - z_0}{2d}\right) \int_0^{2\pi} \left[\frac{g(R',d)}{R'}\right] \left[1 + \frac{2d}{R'}\right] (r - r_0\cos\theta_0) d\theta_0 \\ &\quad - 2(z + z_0)\sinh\left(\frac{z}{2d}\right)\sinh\left(\frac{z_0}{2d}\right) \int_0^{2\pi} \left[\frac{g(R',d)}{R'^2}\right] \left[1 + \frac{6d}{R'} + \frac{12d^2}{R'^2}\right] \\ &\quad (r - r_0\cos\theta_0) d\theta_0, \end{aligned} \tag{28}$$

$$\left[\frac{8\pi\mu}{F}\right]u_z^w(r,z) = -\cosh\left(\frac{z+z_0}{2d}\right)\int_0^{2\pi} g(R',d)d\theta_0$$

$$-(z+z_0)\sinh\left(\frac{z+z_0}{2d}\right)\int_0^{2\pi}\left[\frac{g(R',d)}{R'}\right]\left[1+\frac{2d}{R'}\right]d\theta_0 + 2\sinh\left(\frac{z}{2d}\right)\sinh\left(\frac{z_0}{2d}\right)\times$$

$$\int_0^{2\pi} g(R',d)\left\{1+\frac{2d}{R'}+\frac{4d^2}{R'^2}-\left(\frac{z+z_0}{R'}\right)^2\left[1+\frac{6d}{R'}+\frac{12d^2}{R'^2}\right]\right\}d\theta_0, \qquad (29)$$

$$\left[\frac{8\pi d}{F}\right]p^w(r,z) = -\sinh\left(\frac{z+z_0}{2d}\right)\int_0^{2\pi} g(R',d)d\theta_0$$

$$-(z+z_0)\cosh\left(\frac{z+z_0}{2d}\right)\int_0^{2\pi}\left[\frac{g(R',d)}{R'}\right]\left[1+\frac{2d}{R'}\right]d\theta_0 + 2\cosh\left(\frac{z}{2d}\right)\sinh\left(\frac{z_0}{2d}\right)\times$$

$$\int_0^{2\pi} g(R',d)\left\{1+\frac{2d}{R'}+\frac{4d^2}{R'^2}-\left(\frac{z+z_0}{R'}\right)^2\left[1+\frac{6d}{R'}+\frac{12d^2}{R'^2}\right]\right\}d\theta_0 \qquad (30)$$

in which R' designates the distance between the point $\mathbf{x}$ and the symmetric $\mathbf{x}_0'$ of the point $\mathbf{x}_0$ with respect to the $z=0$ wall Σ. Hence, $\mathbf{x}_0'$ has the Cartesian coordinates $(x_0, y_0, -z_0)$ and the cylindrical coordinates $(r_0, -z_0, \theta_0)$. Accordingly,

$$R' = \left|\mathbf{x}-\mathbf{x}_0'\right| = \left\{r^2+r_0^2-2rr_0\cos\theta_0+(z+z_0)^2\right\}^{1/2}. \qquad (31)$$

It is straightforward and useful to deduce, by inspecting Equations (25)–(26) and (28)–(29), the following basic properties:

Property 1: As expected, both velocity components $u_r = u_r^\infty + u_r^w$ and $u_z = u_z^\infty + u_z^w$ vanish on the no-slip $z=0$ plane wall (make use on this surface of the equalities $z=0$ and $R=R'$).

Property 2: $u_r = u_r^\infty = u_r^w = 0$ on the $r=0$ axis. This is readily obtained by noting that for $r=0$ both R and R' become independent of θ_0.

3.4. Fundamental bounded flow produced by a radial force distribution

For this case, the vector $\mathbf{s} = \mathbf{e}_r(\theta_0)$ depends on the point $\mathbf{x}_0$ located on the ring and the solution (u_r, u_z, p) is provided by Equations (19)–(21). In the absence of the wall (unbounded liquid case), it has been found by Sellier & Aydin (2016) that

$$\left[\frac{8\pi\mu}{F}\right]u_r^\infty(r,z) = 2\cosh\left(\frac{z-z_0}{2d}\right)\int_0^{2\pi} g(R,d)\cos\theta_0 d\theta_0 + \frac{1}{d}\times$$

$$\int_0^{2\pi}\left[\bar{T}_1\left(\frac{R}{d},\frac{z-z_0}{d}\right)\cos\theta_0-\left(\frac{r-r_0\cos\theta_0}{d}\right)\left(\frac{r\cos\theta_0-r_0}{d}\right)\bar{T}_2\left(\frac{R}{d},\frac{z-z_0}{d}\right)\right]d\theta_0, \tag{32}$$

$$\left[\frac{8\pi\mu}{F}\right]u_z^{\infty}(r,z)=\sinh\left(\frac{z-z_0}{2d}\right)\int_0^{2\pi}\left[\frac{g(R,d)}{R}\right]\left[1+\frac{2d}{R}\right](r\cos\theta_0-r_0)d\theta_0, \tag{33}$$

$$\left[\frac{8\pi d}{F}\right]p^{\infty}(r,z)=\cosh\left(\frac{z-z_0}{2d}\right)\int_0^{2\pi}\left[\frac{g(R,d)}{R}\right]\left[1+\frac{2d}{R}\right](r\cos\theta_0-r_0)d\theta_0 \tag{34}$$

with the auxiliary functions $\bar{T}_1$ and $\bar{T}_2$ defined in Appendix A. For the bounded liquid case, the fields u_r, u_z and p are obtained by applying relations (Equations 19–21) with the components (V_{xt}, V_{zt}, Q_t), for $t = x, y$ determined as recently achieved by Sellier (2017). More precisely, these components are available in the work by Sellier (2017), for $t = x$, for both a conducting wall and an insulating wall (this latter case yielding a more complicated solution). Because there is no electrical potential coupled to the fundamental axisymmetric flow (u_r, u_z, p), it is possible in this section to use the results for a conducting wall. In addition, the other components (V_{xy}, V_{zy}, Q_y) are easily gained, still for a conducting wall, by mimicking the procedure described by Sellier (2017), for $t = x$. Curtailing the details and some elementary manipulations, the desired additional quantities (u_r^w, u_z^w, p_r^w) then take the following forms

$$\left[\frac{8\pi\mu}{F}\right]u_r^w(r,z)=-2\cosh\left(\frac{z+z_0}{2d}\right)\int_0^{2\pi}g(R',d)\cos\theta_0 d\theta_0-\frac{1}{d}\times$$

$$\int_0^{2\pi}\left[\bar{T}_1\left(\frac{R'}{d},\frac{z+z_0}{d}\right)\cos\theta_0-\left(\frac{r-r_0\cos\theta_0}{d}\right)\left(\frac{r\cos\theta_0-r_0}{d}\right)\bar{T}_2\left(\frac{R'}{d},\frac{z+z_0}{d}\right)\right]d\theta_0$$

$$-2\sinh\left(\frac{z}{2d}\right)\sinh\left(\frac{z_0}{2d}\right)\left\{2d\int_0^{2\pi}\left[\frac{g(R',d)}{R'}\right]\left[1+\frac{2d}{R'}\right]\cos\theta_0 d\theta_0\right.$$

$$\left.-\int_0^{2\pi}g(R',d)\left[1+\frac{6d}{R'}+\frac{12d^2}{R'^2}\right]\frac{(r-r_0\cos\theta_0)(r\cos\theta_0-r_0)}{R'^2}d\theta_0\right\}, \tag{35}$$

$$\left[\frac{8\pi\mu}{F}\right]u_z^w(r,z) = -\sinh\left(\frac{z-z_0}{2d}\right)\int_0^{2\pi}\left[\frac{g(R',d)}{R'}\right]\left[1+\frac{2d}{R'}\right](r\cos\theta_0 - r_0)d\theta_0$$

$$+2(z+z_0)\sinh\left(\frac{z}{2d}\right)\sinh\left(\frac{z_0}{2d}\right)\int_0^{2\pi}\left[\frac{g(R',d)}{R'^2}\right]\left[1+\frac{6d}{R'}+\frac{12d^2}{R'^2}\right] \quad (36)$$
$$(r\cos\theta_0 - r_0)d\theta_0,$$

$$\left[\frac{8\pi d}{F}\right]p^w(r,z) = -\cosh\left(\frac{z-z_0}{2d}\right)\int_0^{2\pi}\left[\frac{g(R',d)}{R'}\right]\left[1+\frac{2d}{R'}\right](r\cos\theta_0 - r_0)d\theta_0$$

$$+2(z+z_0)\cosh\left(\frac{z}{2d}\right)\sinh\left(\frac{z_0}{2d}\right)\int_0^{2\pi}\left[\frac{g(R',d)}{R'^2}\right]\left[1+\frac{6d}{R'}+\frac{12d^2}{R'^2}\right] \quad (37)$$
$$(r\cos\theta_0 - r_0)d\theta_0.$$

As for the axial distribution case examined in Section 3.3, the velocity components $u_r^\infty, u_r^w, u_z^\infty, u_z^w$ and also $u_r = u_r^\infty + u_r^w$ and $u_z = u_z^\infty + u_z^w$ given by Equations (32)–(33) and (35)–(36) obey the two properties stated after Equation (31). In establishing Property 1 for the radial velocity components, one should first notice from Appendix A the relations $\bar{T}_k(u,v) = \bar{T}_k(u,-v)$, for $k = 1, 2$.

4. Numerical treatment and flow patterns

This section presents the numerical implementation and the velocity and pressure patterns computed for a few values of the circular ring location $z_0 > 0$ and radius $r_0 > 0$.

4.1. Dimensionless quantities. Computation of the encountered integrals

Following Sellier & Aydin (2016), we henceforth use the dimensionless variables $\bar{r} = r/d, \bar{z} = z/d, \bar{R} = R/d, \overline{R'} = R'/d$ and also the normalised quantities

$$\bar{u}_r = \left[\frac{8\pi\mu d}{F}\right]u_r, \quad \bar{u}_z = \left[\frac{8\pi\mu d}{F}\right]u_z, \quad \bar{p} = \left[\frac{8\pi d^2}{F}\right]p. \quad (38)$$

Similar relations are used to also define the normalised flows $(\bar{u}_r^\infty, \bar{u}_z^\infty, \bar{p}^\infty)$ and $(\bar{u}_r^w, \bar{u}_z^w, \bar{p}^w)$. Since discussed and implemented by Sellier & Aydin (2016), the accurate computation of the quantities $(\bar{u}_r^\infty, \bar{u}_z^\infty, \bar{p}^\infty)$ is not addressed here. In contrast, special attention is paid to the calculation of the additional dimensionless flow $(\bar{u}_r^w, \bar{u}_z^w, \bar{p}^w)$. For convenience, we introduce for positive integers m and n, the integrals

$$J'_{mn} = \int_0^{2\pi} [\overline{R'}]^{-m} \mathrm{e}^{-\overline{R'}/2} (\cos\theta_0)^n d\theta_0, \tag{39}$$

$$J' = \int_0^{2\pi} \{\bar{T}_1(\overline{R'}, \bar{z} + \bar{z}_0)\cos\theta_0$$

$$- (\bar{r} - \bar{r}_0\cos\theta_0)(\bar{r}\cos\theta_0 - \bar{r}_0)\bar{T}_2(\overline{R'}, \bar{z} + \bar{z}_0)\} d\theta_0. \tag{40}$$

Such notations make possible to rewrite the results of Equations (28)–(30) and (32)–(34). It is easily found that:

(i) For the additional flow obtained for the axial force distribution

$$\bar{u}_r^w = -\sinh\left(\frac{\bar{z} - \bar{z}_0}{2}\right)\{(J'_{20} + 2J'_{30})\bar{r} - (J'_{21} + 2J'_{31})\bar{r}_0\} - 2(\bar{z} + \bar{z}_0) \times$$

$$\sinh\left(\frac{\bar{z}}{2}\right)\sinh\left(\frac{\bar{z}_0}{2}\right)\{(J'_{30} + 6J'_{40} + 12J'_{50})\bar{r} - (J'_{31} + 6J'_{41} + 12J'_{51})\bar{r}_0\}, \tag{41}$$

$$\bar{u}_z^w = -\cosh\left(\frac{\bar{z} + \bar{z}_0}{2}\right)J'_{10} - (\bar{z} + \bar{z}_0)\sinh\left(\frac{\bar{z} + \bar{z}_0}{2}\right)(J'_{20} + 2J'_{30})$$

$$+ 2\sinh\left(\frac{\bar{z}}{2}\right)\sinh\left(\frac{\bar{z}_0}{2}\right)\{(J'_{10} + 2J'_{20} + 4J'_{30}) - (\bar{z} + \bar{z}_0)^2(J'_{30} + 6J'_{40} + 12J'_{50})\}, \tag{42}$$

$$\bar{p}^w = -\sinh\left(\frac{\bar{z} + \bar{z}_0}{2}\right)J'_{10} - (\bar{z} + \bar{z}_0)\cosh\left(\frac{\bar{z} + \bar{z}_0}{2}\right)(J'_{20} + 2J'_{30})$$

$$+2\cosh\left(\frac{\bar{z}}{2}\right)\sinh\left(\frac{\bar{z}_0}{2}\right)\{(J'_{10} + 2J'_{20} + 4J'_{30}) - (\bar{z} + \bar{z}_0)^2(J'_{30} + 6J'_{40} + 12J'_{50})\}. \tag{43}$$

(ii) For the additional flow obtained for the radial force distribution

$$\bar{u}_r^w = -2\cosh\left(\frac{\bar{z} + \bar{z}_0}{2}\right)J'_{11} - J' - 2\sinh\left(\frac{\bar{z}}{2}\right)\sinh\left(\frac{\bar{z}_0}{2}\right) \times$$

$$\{(J'_{32} + 6J'_{42} + 12J'_{52})\bar{r}\bar{r}_0 - (J'_{31} + 6J'_{41} + 12J'_{51})(\bar{r} + \bar{r}_0)\bar{r}$$

$$+ (J'_{30} + 6J'_{40} + 12J'_{50})\bar{r}^2 + 2(J'_{21} + 2J'_{31})\}, \tag{44}$$

$$\bar{u}_z^w = -\sinh\left(\frac{\bar{z}-\bar{z}_0}{2}\right)\{(J'_{21}+2J'_{31})\bar{r}-(J'_{20}+2J'_{30})\bar{r}_0\}+2(\bar{z}+\bar{z}_0)\times$$

$$\sinh\left(\frac{\bar{z}}{2}\right)\sinh\left(\frac{\bar{z}_0}{2}\right)\{(J'_{31}+6J'_{41}+12J'_{51})\bar{r}-(J'_{30}+6J'_{40}+12J'_{50})\bar{r}_0\}, \tag{45}$$

$$\bar{p}^w = -\cosh\left(\frac{\bar{z}-\bar{z}_0}{2}\right)\{(J'_{21}+2J'_{31})\bar{r}-(J'_{20}+2J'_{30})\bar{r}_0\}+2(\bar{z}+\bar{z}_0)\times$$

$$\cosh\left(\frac{\bar{z}}{2}\right)\sinh\left(\frac{\bar{z}_0}{2}\right)\{(J'_{31}+6J'_{41}+12J'_{51})\bar{r}-(J'_{30}+6J'_{40}+12J'_{50})\bar{r}_0\}. \tag{46}$$

Accordingly, the numerical implementation must examine at which accuracy level the integrals J' and J_{mn}, occurring in Equations (41)–(46), are calculated. Setting $\alpha = \theta_0/2$, the integral J' becomes

$$J' = 4\int_0^{\pi/2}\{\bar{T}_1(u,v)\cos 2\alpha-(\bar{r}-\bar{r}_0\cos 2\alpha)(\bar{r}\cos 2\alpha-\bar{r}_0)\bar{T}_2(u,v)\}d\alpha, \tag{47}$$

with $v=\bar{z}+\bar{z}_0>0$ and $u=\overline{R'}\geq v$ since $\overline{R'}^2-v^2=(\bar{r}-\bar{r}_0)^2+2(1-\cos 2\alpha)$. The integral J' is computed in Fortran using, for α in $[0,\pi/2]$, a Gaussian-Legendre quadrature. A few Gauss points are needed whenever $|\bar{r}-\bar{r}_0|$ is not too small. In contrast (recall the definitions of $\bar{T}_1$ and $\bar{T}_2$ given in Appendix A), as $\bar{r}$ approaches $\bar{r}_0$ more and more Gauss points are needed and the approximation of J' becomes of poor quality even with a very large number of Gauss points when $v>0$ is of order unity or larger. This trend is illustrated, taking $\bar{r}=\bar{r}_0$, in the third column of Table 1.

Actually, it turns out that $u\to v$ when both $\bar{r}-\bar{r}_0$ and α vanish. Then, the first and third terms on the right-hand side of the definition (Equation (57)) of $\bar{T}_1(u,v)$ become singular, while the sum of these terms remains finite (for $\bar{T}_2(u,v)$ a similar remark holds for three terms in Equation (58)). This suggests resorting for $\bar{T}_1$ and $\bar{T}_2$ to the more suitable and equivalent forms (Equations 59–60) built for $v>0$. As illustrated in Table 1, using this trick for the term $\bar{T}_1$ makes possible to accurately compute the integral J' even with a double precision Fortran code. Even with the double precision code, there is no need to take the equivalent form (Equation (60)) for the term $\bar{T}_2$. This is because it appears in Equation (47) with the regularising factor $(\bar{r}-\bar{r}_0\cos 2\alpha)(\bar{r}\cos 2\alpha-\bar{r}_0)=(\bar{r}_0)^2(1-\cos 2\alpha)^2$. Note that for the quadruple precision Fortran code using Equations (57) and (58) yields accurate results.

Table 1. Computed integral J' for $\bar{r} = \bar{r}_0 = 1$ and a few values of $v = \bar{z} + \bar{z}_0 > 0$. The last column provides the results obtained using the Mathematica Sofware. For other columns of results, the Fortran Code is used with an indication of the terms $\bar{T}_k$ (taking $k = 1$ and/or $k = 2$) for which the equivalent forms (Equations 59–60) are employed. The Fortran code precision, either double (D) or quadruple (Q), is given in the second column.

v	A	None	$\bar{T}_1$	$\bar{T}_2$	$\bar{T}_1, \bar{T}_2$	Mathematica
1	D	−1.8270971208	−1.8270971120	−1.8270971202	−1.8270971120	−1.8270971120
1	Q	−1.8270971120	−1.8270971120	−1.8270971120	−1.8270971120	−1.8270971120
5	D	−0.1026961957	−0.1030576147	−0.1026961957	−0.1030576147	−0.1030576147
5	Q	−0.1030576147	−0.1030576147	−0.1030576147	−0.1030576147	−0.1030576147
10	D	57,092.728231	−0.0212132027	57,092.728231	−0.0212132027	−0.0212132027
10	Q	−0.0212132027	−0.0212132027	−0.0212132027	−0.0212132027	−0.0212132027
30	D	−433,997.18829	−0.0019511366	−433,997.18829	−0.0019511371	−0.0019511371
30	Q	−0.0019511371	−0.0019511371	−0.0019511371	−0.0019511371	−0.0019511371

In implementing relations (Equations (41)–(46)), it is also necessary to accurately compute the integrals J'_{mn} defined by Equation (39), for $m = 1, ..., 5$ (taking $n = 0, 1$ if $m = 0, 1$ and $n = 0, 1, 2$ if $m = 3, ..., 5$). Definition (Equation (31)) of $R' = d(\overline{R'})$ suggests that accuracy troubles might occur in the evaluation of J'_{mn} for points $(\bar{r}, \bar{z})$ close to the normalised trace $(\bar{r}_0, -\bar{z}_0)$ of the symmetric of the ring with respect to the solid $z = 0$ plane wall. To investigate this issue, we mimick Sellier & Aydin (2016) and introduce the auxiliary integrals I'_{mn} as follows:

$$I'_{mn} = \int_0^{2\pi} [\overline{R'}]^{-m} (\cos\theta_0)^n d\theta_0. \tag{48}$$

When $(\bar{r}, \bar{z})$ approaches $(\bar{r}_0, -\bar{z}_0)$, it becomes useful to recast J'_{mn} in terms of some integrals I'_{mn} and of another extra integral easy to compute accurately. For instance, J'_{5n} is rewritten as follows:

$$J'_{5n} = \int_0^{2\pi} [\overline{R'}]^{-5} \left\{ e^{-\overline{R'}/2} - 1 + \overline{R'}/2 - \overline{R'}^2/8 + \overline{R'}^3/48 - \overline{R'}^4/384 \right\} (\cos\theta_0)^n d\theta_0$$

$$+ I'_{5n} - I'_{4n}/2 + I'_{3n}/8 - I'_{2n}/48 + I'_{1n}/384, \tag{49}$$

For $m = 1, ..., 4$, a decomposition similar to Equation (49) for J'_{mn} is also easily obtained (it involves the integrals I'_{kn} with $k = 1, ..., m$). Clearly, there is no difficulty in computing accurately the first integral on the right-hand side of Equation (49) when $(\bar{r}, \bar{z})$ becomes close to $(\bar{r}_0, -\bar{z}_0)$. The task then reduces to the accurate computation of each integral I'_{mn} which, taking $\omega = (\pi - \theta_0)/2$, also reads as

$$I'_{mn} = \frac{4k'^m}{(4\bar{r}\bar{r}_0)^{m/2}} \int_0^{\pi/2} \frac{(2\sin^2\omega - 1)^n d\omega}{(1 - k'^2 \sin^2\omega)^{m/2}}, \quad k' = \left[\frac{4\bar{r}\bar{r}_0}{(\bar{r} + \bar{r}_0)^2 + (\bar{z} + \bar{z}_0)^2} \right]^{1/2}. \tag{50}$$

Note that $0 < k' < 1$ for $\bar{r}\bar{r}_0 \neq 0$. Moreover, by virtue of Equation (50), accuracy troubles might arise for the calculation of I'_{mn} when $k'^2 \to 1$. For given $(\bar{r}_0, \bar{z}_0)$, it appears that k'^2 reaches its largest value ${k'_{max}}^2$ for $\bar{z} = 0$ and $\bar{r} = \{\bar{r}_0^2 + \bar{z}_0^2\}^{1/2}$. As may be checked by the reader, ${k'_{max}}^2$ solely depends upon the ratio $\bar{\gamma} = \bar{z}_0/\bar{r}_0$ and takes the value ${k'_{max}}^2 = 2/[1 + (1 + \bar{\gamma}^2)^{1/2}]$.

In summary, accuracy troubles in the computation of the integrals I'_{mn} and, therefore, also the integrals J'_{mn} from the definitions (Equation (39)) might occur at $\bar{z} = 0$ and $\bar{r} = \bar{r}_c(\bar{\gamma}) = \bar{r}_0[1 + \bar{\delta}^2]^{1/2}$ when $\bar{\gamma} = \bar{z}_0/\bar{r}_0 \to 0$. This basic issue has been investigated by computing the integrals J'_{mn} for a few small values of $\bar{\gamma}$ and $(\bar{r}, \bar{z}) = (\bar{r}_c(\bar{\gamma}), 0)$. More precisely, it is achieved, using Equation (39) and performing the change of variable $\omega = (\pi - \theta_0)/2$. The numerical evaluation of the integral is then performed with either the Mathematica Software or a quadruple precision Fortran code by choosing N_G Gauss-Legendre points in the interval $[0, \pi/2]$.

The results are displayed in Table 2 for the most tricky case $m = 5$, taking $\bar{r}_0 = 1$ and $n = 0$. The number N_G of Gaussian points which is large enough to reach a good accuracy, is given (N_G has been found to be independent of the value of $n = 0, 1, 2$). As seen in Table 2, it has been found that the results are excellent for $\bar{\gamma} = \bar{z}_0/\bar{r}_0 = z_0/r_0 \geq 0.001$. This range of location $z_0 \geq (0.001)r_0$, for a given circular ring of radius r_0, is quite sufficient for the intended future application of the present work to the motivating problem presented in Section 2.1. Accordingly, in this work, each integral J'_{mn} is computed directly from its definition (Equation (39)), i.e. no use is made of a decomposition analogous to Equation (49).

In view of the accuracy issues previously discussed in this subsection, each encountered fundamental flow quantities (velocity components, pressure) has been computed in the present work using a quadruple precision Fortran code.

4.2. Flow velocity and pressure patterns

For comparison purposes, a few isolevel curves have been computed for the dimensionless (recall Equation (38)) bounded fundamental flow $(\bar{u}_r, \bar{u}_z, \bar{p})$

Table 2. Computed integral J'_{50} for $\bar{r}_0 = 1$ and different values of the normalised ring location $\bar{\gamma} = \bar{z}_0$. The quantity J'_{50} is calculated from its definition (Equation (39)), taking $\bar{z} = 0$ and $\bar{r} = \bar{r}_0[1 + \bar{\gamma}^2]^{1/2}$ and applying the change of variable $\omega = (\pi - \theta_0)/2$. Use is made of the Mathematica Software of a quadruple precision Fortran code spreading N_G Gaussian points over the domain $[0, \pi/2]$ in ω..

$\bar{\gamma}$	Mathematica	Fortran Code	N_G
0.1	12,485.481502534	12,485.481502523	64
0.01	132,541,302.39429	132,541,302.39429	128
0.001	1,332,547,268,831.9	1,332,547,268,832.2	512

and unbounded fundamental flow $(\bar{u}_r^{\infty}, \bar{u}_z^{\infty}, \bar{p}^{\infty})$. The obtained results obtained depend upon the circular ring force distribution (axial or radial one), normalised radius $\bar{r}_0$ and location $\bar{z}_0$. For conciseness, the attention is however restricted in this subsection to the choices $\bar{r}_0 = \bar{z}_0 = 1$. Accordingly, the trace of the ring is located at the point $(\bar{r}, \bar{z}) = (1, 1)$ in the truncated domain of the liquid displayed in the figures below.

The results for the axial velocity component are displayed in Figure 2. For the axial force distribution, $\bar{u}_z^{\infty}$ is slightly different from zero at $\bar{z} = 0$. Consequently, $\bar{u}_z$ (which vanishes on the $\bar{z} = 0$ wall) is seen (compare Figure 2(a) to Figure 2(b)) to be very different from $\bar{u}_z^{\infty}$ in the entire reported domain $\bar{z} \leq 4$. Not surprisingly, for the radial force distribution on the ring, the axial velocity is much smaller than the one produced by the axial force distribution. This property holds for both bounded and unbounded fundamental flows. As a consequence, for the radial force distribution, $\bar{u}_z$ and $\bar{u}_z^{\infty}$ are very close together for $\bar{r} \geq O(2)$. In contrast, these quantities are very different in the domain $\bar{r} \leq O(2)$ in which ring–wall interactions therefore strongly affect the unbounded fundamental flow.

The counterpart of Figure 2 for the dimensionless radial velocity component is shown in Figure 3. This quantity is seen to be deeply affected by the wall–ring interactions for both force distributions (axial or radial). This is especially clear when comparing for the unbounded and the bounded flows the domains in which the radial velocity remains positive. Contrary to the case of the axial velocity component illustrated in Figure 2, the wall–ring interactions are found to quickly decay away from the wall (becoming here of small magnitude as soon as $\bar{z} \geq O(2)$) for both force distributions. Due to the requirement of a zero velocity on the no-slip wall, the wall–ring interactions are strong near the wall, i.e. here in the $\bar{z} \leq O(2)$ domain, whatever the force distribution on the ring.

Comparisons for the normalised fundamental pressure fields obtained for the unbounded and bounded flows are given in Figure 4. Large wall–ring interactions are seen to occur for the axial force distribution in the entire liquid domain. This is also the case for the radial force distribution except sufficiently away from the wall, i.e. here for $\bar{z} \geq O(2)$. These trends are again clear when comparing the location of the zero pressure contours obtained for the different fundamental flows.

4.3. Flow streamlines

In the previous subsection, wall–ring interactions have been found to affect the fundamental axial and radial velocity components, especially near the $\bar{r} = 0$ axis and for $\bar{z} \leq O(2)$. However, each velocity component experiences its own dependence and it is therefore useful to also investigate the velocity streamlines when discussing each (axial or radial force distribution)

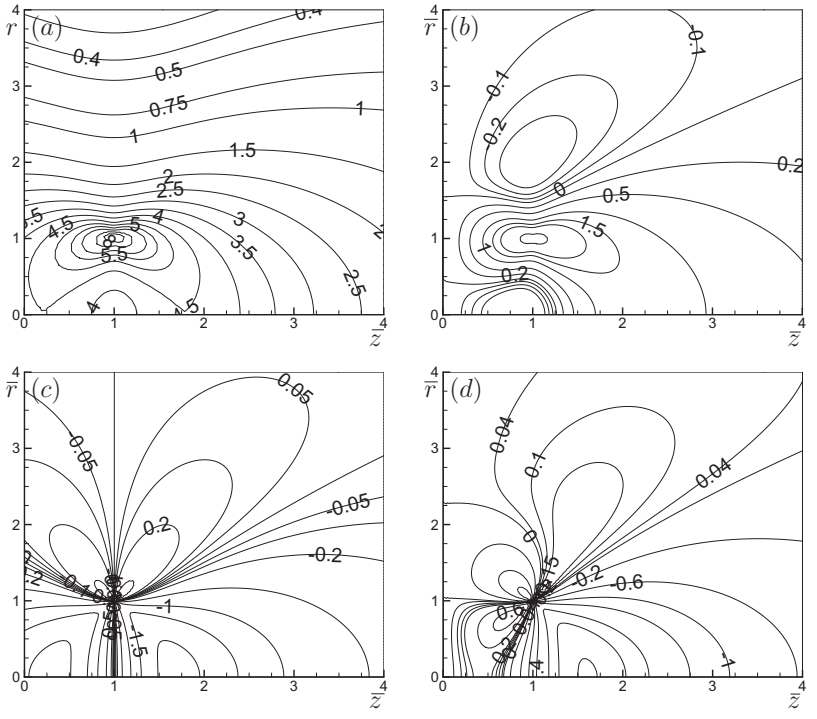

Figure 2. Isolevel contours of the normalised axial velocity component for $\bar{r}_0 = \bar{z}_0 = 1$. $\bar{u}_z^{\infty}$ (a) and $\bar{u}_z$ (b) are for the axial force distribution while $\bar{u}_z^{\infty}$ (c) and $\bar{u}_z$ (d) are for the radial force distribution.

fundamental flow field sensitivity to the liquid domain nature (unbounded or bounded). Note that the fundamental flow $\mathbf{u}$ has the same streamlines as its normalised counter-part flow with velocity components $(\bar{u}_r, \bar{u}_z)$.

As in Section 4.2, we first take $\bar{r}_0 = \bar{z}_0 = 1$ and draw the associated streamlines in Figure 5. Comparing the streamlines obtained for the unbounded and the bounded fundamental flows reveals that wall–ring interactions strongly affect the fundamental flows in the *entire* liquid domain whatever the force distribution nature (axial or radial one) spread on the ring. For instance, for the axial force distribution, the flow field $\mathbf{u}$ exhibits in Figure 5(b) *closed* streamlines while it is not the case for $\mathbf{u}^{\infty}$ in Figure 5(a). As a consequence of Figure 5(b), fluid particles located near both the no-slip wall and the $\bar{r}_0 = 0$ axis are trapped. For the radial force distribution, only open streamlines are found for $\mathbf{u}$ in Figure 5(d) while some closed streamlines exit for $\mathbf{u}^{\infty}$ in Figure 5(c). In addition, one should note the occurrence in Figure 5(d) of a stagnation point (i.e. where $\mathbf{u} = 0$) located at $(\bar{r}, \bar{z}) \sim (2.2, 0.6)$.

Finally, the $\bar{r}_0 = 1$ circular ring is approached to the wall taking henceforth $\bar{z}_0 = 0.1$. The streamlines computed for this new ring location are given in Figure 6. Clearly, these streamlines strongly differ from those obtained in Figure 5 for $\bar{z}_0 = 1$.

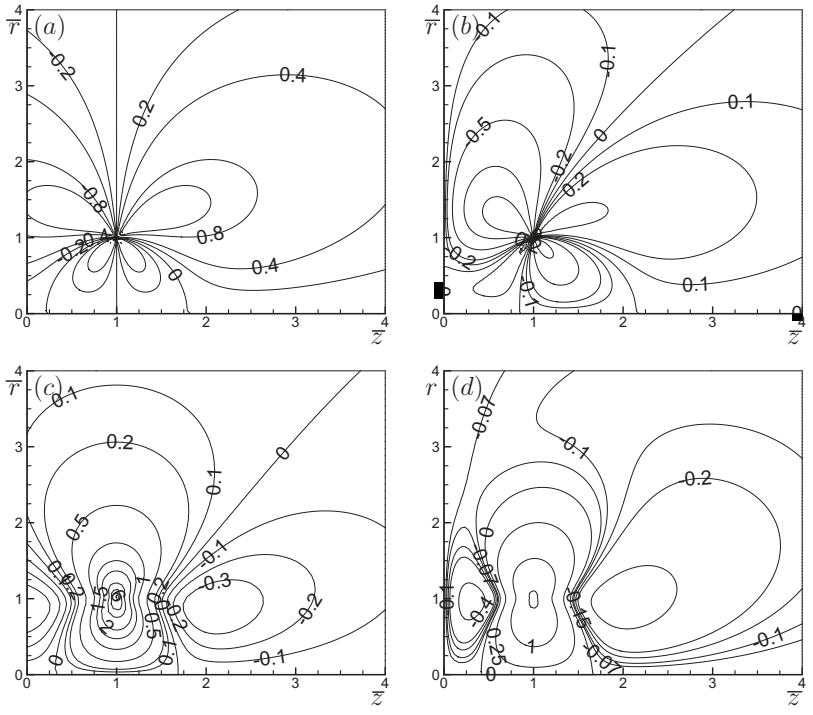

Figure 3. Isolevel contours of the normalised radial velocity component for $\bar{r}_0 = \bar{z}_0 = 1$. $\bar{u}_r^{\infty}$ (a) and $\bar{u}_r$ (b) are for the axial force distribution while $\bar{u}_r^{\infty}$ (c) and $\bar{u}_r$ (d) are for the radial force distribution.

5. Application to the case of a solid sphere translating normal to the wall

This section deals with the problem of a solid sphere translating normal to the wall. More precisely, it shows how to get the local traction applied on the sphere boundary by resorting to a boundary approach in which the previous fundamental flows play a key role.

5.1. Advocated boundary representations and related boundary-integral equations

As shown in Figure 1, we consider a solid sphere, with radius a and surface S, translating normal to the wall at the velocity $U\mathbf{e}_z$. There is no electric field ϕ (see Section 2.2) and the axisymmetric flow about the sphere has velocity $\mathbf{u}(\mathbf{x}) = u_r(r,z)\mathbf{e}_r + u_z(r,z)\mathbf{e}_z$ and pressure $p(\mathbf{x}) = p(r,z)$ governed by Equation (1) with $\phi = 0$ and Equation (3) with $\mathbf{u}_{rb} = U\mathbf{e}_z$. On the sphere boundary, the surface traction $\mathbf{f} = \sigma.\mathbf{n}$ reads $\mathbf{f} = f_r(r,z)\mathbf{e}_r + f_z(r,z)\mathbf{e}_z$. For symmetries reasons, the sphere experiences a zero torque about its centre O' and a force $\mathbf{F}$ given by

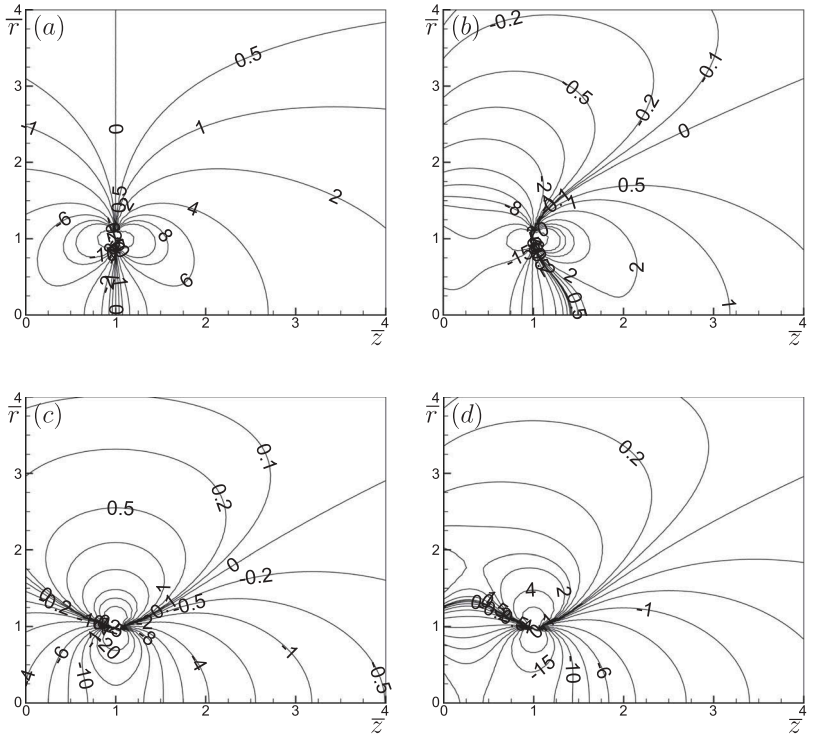

Figure 4. Isolevel contours of the normalised pressure for $\bar{r}_0 = \bar{z}_0 = 1$. $\bar{p}^{\infty}$ (a) and $\bar{p}$ (b) are for the axial force distribution while $\bar{p}^{\infty}$ (c) and $\bar{p}$ (d) are for the radial force distribution.

$$\mathbf{F} = \int_S \mathbf{f} dS = [2\pi \int_C f_z(P) r(P) dl(P)] \mathbf{e}_z = -6\pi\mu a \lambda U \mathbf{e}_z \tag{51}$$

where $\mathcal{C}$ is the half-circle trace of S in the $\theta = 0$ half plane and $\lambda > 0$ the so-called drag coefficient. Note that in Equation (51), each point P lies on $\mathcal{C}$ and has cylindrical coordinates $r(P), z(P)$ and $\theta(P) = 0$.

As done by Sellier & Aydin (2017) for the unbounded liquid, we can actually resort to two different boundary formulations to get the traction $\mathbf{f}$ on the sphere surface. The first one, further denoted M1, appeals to the fundamental axisymmetric MHD flow produced in an *unbounded* liquid by distributing on the ring with radius $r_P > 0$ and location $z = z_P$ point forces with strength $F_r \mathbf{e}_r + F_z \mathbf{e}_z$ and (F_r, F_z) constant. This basic flow is without swirl and its pressure $q(\mathbf{x}) = q(r, z)$ and velocity $\mathbf{v}(\mathbf{x}) = v_r(r, z)\mathbf{e}_r + v_z(r, z)\mathbf{e}_z$ have been analytically determined by Sellier & Aydin (2016). Introducing points $M(r, z)$ and $P(r_P, z_P)$ in the half $\theta = 0$ plane, taking indices α and β in $\{r, z\}$ and adopting henceforth the usual tensor summation convention yields

$$v_\alpha(\mathbf{x}) = \left[\frac{1}{8\pi\mu}\right] G^{\infty}_{\alpha\beta}(M, P) F_\beta \text{ for } M \neq P \tag{52}$$

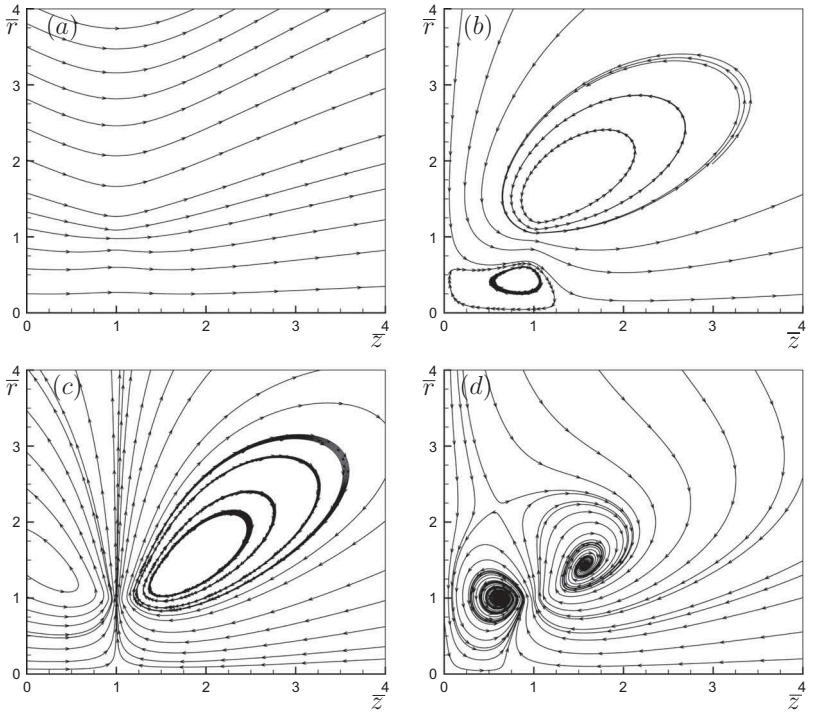

Figure 5. Unbounded and bounded fundamental flows streamlines for $\bar{r}_0 = \bar{z}_0 = 1$. Both axial force distribution (unbounded flow (a) and bounded flow (b)) and radial force distribution (unbounded flow (c) and bounded flow (d)) on the circular ring are considered.

with so-called free-space Green velocity tensor components $G^{\infty}_{\alpha\beta}(M,P)$ expressed versus $(z - z_P, r, r_P, d)$ in the work by Sellier & Aydin (2017). Mimicking the procedure worked out by Pozrikidis (1992) for the $\mathrm{Ha} = 0$ Stokes flow case then provides for the velocity $\mathbf{u}$ about the sphere the integral representation

$$u_\alpha(\mathbf{x}) = -\frac{1}{8\pi\mu}\int_{\mathcal{C}\cup\mathcal{L}} G^{\infty}_{\alpha\beta}(M,P) f_\beta(P) r(P) dl(P) \text{ for } \mathbf{x} \in \mathcal{D}\cup S\cup\Sigma, \qquad (53)$$

where the unbounded straight line $\mathcal{L}$ denotes the trace of Σ in the $\theta = 0$ half plane.

In a similar manner, we can deduce from the previous sections the fundamental axisymmetric MHD flow having a vanishing velocity on the $z = 0$ wall Σ and produced in the *bounded* $z > 0$ liquid domain by distributing on the ring with radius $r_P > 0$ and location $z = z_P > 0$ point forces with strength $F_r\mathbf{e}_r + F_z\mathbf{e}_z$ and (F_r, F_z) constant. This second flow velocity and pressure read as in Equation (52) with previous free-space components $G^{\infty}_{\alpha\beta}$ and $P^{\infty}_{\beta}(M,P)$ replaced by components $G^{wall}_{\alpha\beta}$ and $P^{wall}_{\beta}(M,P)$ obtained from Section 3.3 and Section 3.4. As a result, $G^{wall}_{\alpha\beta}(M,P) = G^{wall}_{\beta\alpha}(P,M)$.

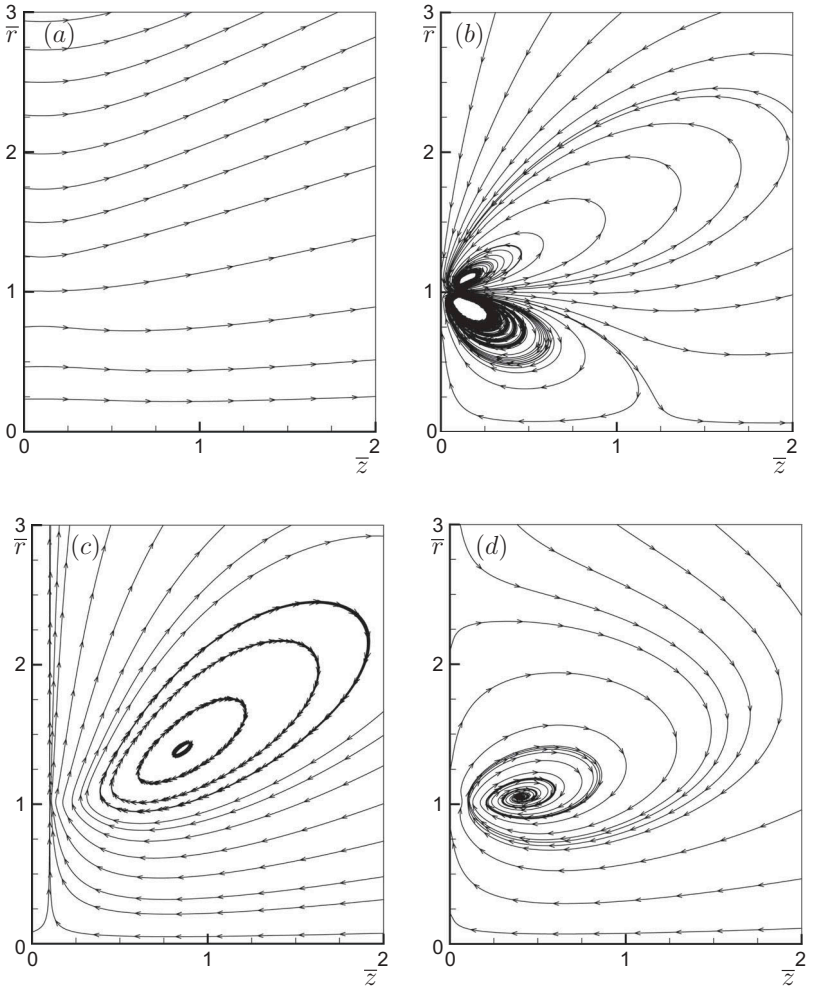

Figure 6. Unbounded and bounded fundamental flows streamlines for $\overline{r}_0 = 1$ and $\overline{z}_0 = 0.1$. Both axial force distribution (unbounded flow (a) and bounded flow (b)) and radial force distribution (unbounded flow (c) and bounded flow (d)) on the circular ring are considered.

Moreover, by essence $G^{wall}_{\alpha\beta}(M,P) = 0$ for $z = 0$. Consequently, the counterparts of Equation (53) for this second boundary-approach, termed M2, is

$$u_\alpha(\mathbf{x}) = -\frac{1}{8\pi\mu}\int_{\mathcal{C}} G^{wall}_{\alpha\beta}(M,P) f_\beta(P) r(P) dl(P) \text{ for } \mathbf{x} \in \mathcal{D} \cup S \cup \Sigma. \tag{54}$$

In summary, Equations (53) and (54) are single-layer boundary integral representations of the required flow velocity $\mathbf{u}$ about the sphere for M1 (free-space fundamental flow) and M2 (wall-bounded fundamental flow), respectively. Enforcing the velocity boundary conditions (Equation (3)) on $S \cup \Sigma$ now results in boundary-integral equations for the unknown traction $\mathbf{f} = f_r(r,z)\mathbf{e}_r + f_z(r,z)\mathbf{e}_z$ on $\mathcal{C} \cup \mathcal{L}$ for M1 and on $\mathcal{C}$ for M2 (for which the

condition $\mathbf{u} = 0$ at $z = 0$ is already satisfied from Equation (54) in virtue of the previously noticed property $G^{wall}_{\alpha\beta}(M,P) = 0$ for $z = 0$). Denoting by δ the usual Kronecker symbol, these boundary-integral equations are

$$\int_{\mathcal{C}\cup\mathcal{L}} G^{\infty}_{\alpha\beta}(M,P) f_\beta(P) r(P) dl(P) = -8\pi\mu U \delta_{\alpha z} \text{ for } M \in \mathcal{C}\cup\mathcal{L} \text{ in } M1, \quad (55)$$

$$\int_{\mathcal{C}} G^{wall}_{\alpha\beta}(M,P) f_\beta(P) r(P) dl(P) = -8\pi\mu U \delta_{\alpha z} \delta(M,\mathcal{C}) \text{ for } M \in \mathcal{C} \text{ in } M2 \quad (56)$$

with $\delta(M,\mathcal{C}) = 1$ if M is belongs to $\mathcal{C}$ and $\delta(M,\mathcal{C}) = 0$ otherwise. In summary, for M1 or M2 one obtains the traction $\mathbf{f}$ on $\mathcal{C}$ by inverting Equation (55) or Equation (56).

5.2. Numerical results

As in Sellier & Aydin (2017), quadratic 3-node boundary elements are used to discretise the half-circle contour $\mathcal{C}$ and also for M1 the truncated line $\mathcal{L}$ (it is truncated beyond $r = L$). Equally sized elements are used on $\mathcal{C}$ while both elements of equal or unequal lengths have been employed in M1 for the truncated line $\mathcal{L}$. The traction on the sphere surface is then obtained by inverting either Equation (55) or Equation (56) and this permits one to compute the normalised drag coefficient λ (see Equation (51)) versus the sphere centre distance to the wall l and the Hartmann number Ha.

The convergence of the computed drag coefficient versus the method ($M1$ or $M2$) and the number N of nodal points on $\mathcal{C}$ for different Ha and a close sphere with $l/a = 1.1$ is reported in Table 3.

Clearly, for a given value of Ha the predictions of M1 and M2 converge as N increases. Moreover, taking M2 with $N = 60$ is sufficient to ascertain a good accuracy level in the domain $l/a \geq 1.1$ and Ha ≤ 10. Other values $2 \leq L/a \leq 5$ have been tested and found to provide very close results. From the previous results, the drag coefficient has been computed using M2 with $N = 60$ for different sphere normalised location $l/a \geq 1.1$ and Hartmann number Ha ≤ 10.

The results are displayed in Figure 7. Not surprisingly and as for the Ha $= 0$ pure Stokes flow case, the drag coefficient increases slightly for a given Hartmann number as the sphere approaches the wall. Moreover, for a given sphere location, increasing Ha (i.e. for a given liquid increasing the magnitude of the ambient magnetic field) results beyond Ha$\sim$1 in a large increase of the drag experienced by the translating sphere.

Table 3. Computed drag coefficients λ versus the number N of nodal points on $\mathcal{C}$ (indicated in parenthesis) and the employed method for a close sphere with $l/a = 1.1$. For $M1$ the truncature length is $L = 5a$ whatever Ha.

Ha	M2(20)	M1(20)	M2(40)	M1(40)	M2(60)	M1(60)	M2(80)	M1(80)
0.1	11.483	11.502	11.472	11.480	11.469	11.473	11.468	11.470
1	11.742	11.762	11.730	11.740	11.727	11.733	11.726	11.730
10	24.818	24.915	24.791	24.855	24.783	24.837	24.779	24.828

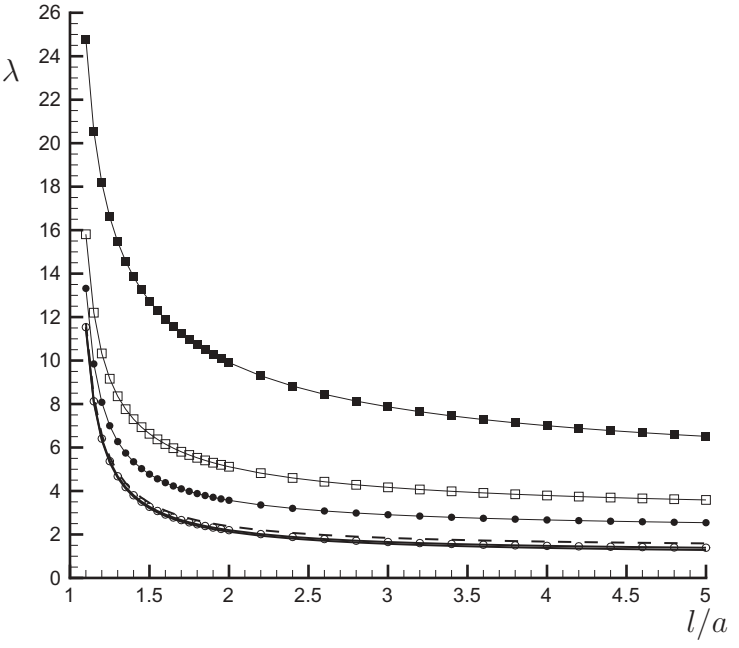

Figure 7. Computed drag coefficient λ versus $l/a \geq 1$ for Ha = 0.01 (solid line), Ha = 0.5(○), Ha = 1 (dashed line), Ha = 3(●), Ha = 5(□) and Ha = 10(■).

6. Concluding remarks

Two different fundamental axisymmetric MHD flows of a conducting liquid bounded by a no-slip motionless insulating or perfectly conducting wall have been determined and computed in this work. More precisely, the wall is normal to the ambient uniform magnetic field and the considered flows, due to a radial or axial distribution of forces on a circular ring, are built by appealing to the three-dimensional fundamental flow produced by a source point obtained analytically by Sellier (2017). As a consequence, the pressure and also both the axial and the radial velocity components of each axisymmetric fundamental flow have been expressed in terms of one-dimensional integrals. The accurate computation of these integrals makes it possible to examine each fundamental flow pattern. As shown by comparing the computed fundamental flows for the considered bounded liquid case and for the unbounded liquid case treated by Sellier & Aydin

(2016), wall–ring interactions are found to deeply affect each fundamental flow (i.e. for both the axial and the radial force distribution on the ring) whenever the circular ring radius is larger or of order of the ring–wall gap. This result clearly appears when paying attention to the streamlines. In contrast and although not shown in the paper for conciseness reasons, weak wall–ring interactions have been also, and not surprisingly, observed for wall–ring gaps large compared to the ring radius.

The derived fundamental axisymmetric flows have also been used to determine the drag experience by a solid sphere translating normal to the wall. This has been done by employing a boundary formulation in which those flows play a key role. Our computations reveal that the drag exerted on the sphere is deeply sensitive to the sphere–wall gap and the Hartmann number.

In future it would be nice to also cope with non-spherical translating bodies of revolution (see Section 2.2) and to also investigate the resulting MHD velocity and pressure fields in the bounded liquid. Such a challenging task is postponed to another work.

Disclosure statement

No potential conflict of interest was reported by the authors.

References

Branover, G. G., & Tsinober, A. B. (1970). *Magnetohydrodynamic of incompressible media*. Moscow: Nauka.

Chester, W. (1957). The effect of a magnetic field on Stokes flow in a conducting fluid. *Journal of Fluid Mechanics*, *3*, 304–308.

Chester, W. (1961). The effect of a magnetic field on the flow of a conducting fluid past a body of revolution. *Journal of Fluid Mechanics*, *10*, 459–465.

Gotoh, K. (1960). Stokes flow of an electrically conducting fluid in a uniform magnetic field. *Journal of the Physical Society of Japan*, *15*(4), 696–705.

Hartmann, J. (1937). Theory of the laminar flow of an electrically conductive liquid in a homogeneous magnetic field. *Det Kgl. Danske Videnskabernes Selskab. Mathematisk-fysiske Meddelelser*, *XV*(6), 1–28.

Moreau, R. (1990). MagnetoHydrodynamics. In *Fluid mechanics and its applications*. Dordrecht: Kluwer Academic Publisher.

Pozrikidis, C. (1992). *Boundary integral and singularity methods for linearized viscous flow*. Cambridge: Cambridge University Press.

Priede, J. (2013). Fundamental solutions of MHD Stokes flow. *arXiv: 1309.3886v1. Physics Fluid Dynamics*.

Sellier, A. (2017). Fundamental MHD creeping flow bounded by a motionless plane solid wall. *European Journal of Computational Mechanics*, 26(4), 411–429.

Sellier, A., & Aydin, S. H. (2016). Fundamental free-space solutions of a steady axisymmetric MHD viscous flow. *European Journal of Computational Mechanics*, *25*(1–2), 194–217.

Sellier, A., & Aydin, S. H. (2017). Creeping axisymmetric MHD flow about a sphere translating parallel with a uniform ambient magnetic field. *MagnetoHydrodynamics*, *53*(1), 5–14.

Tsinober, A. B. (1970).MHD flow around bodies. In *Fluid mechanics and its applications*. Riga: Kluwer Academic Publisher.

Appendix A. *Auxiliary functions* $\bar{T}_1$ *and* $\bar{T}_2$

The functions $\bar{T}_1$ and $\bar{T}_2$ are defined for $u \neq 0$ and $u^2 \neq v^2$ as follows (see Sellier & Aydin (2016))

$$\bar{T}_1(u,v) = \frac{1}{u}\left\{\frac{e^{-(u-v)/2}}{u-v} + \frac{e^{-(u+v)/2}}{u+v}\right\} - \frac{2}{u^2-v^2}, \tag{57}$$

$$\bar{T}_2(u,v) = \frac{1}{u^2}\left\{\left[\frac{u+2}{2u}\right]\left[\frac{e^{-(u-v)/2}}{u-v} + \frac{e^{-(u+v)/2}}{u+v}\right]\right.$$

$$\left. + \frac{e^{-(u-v)/2}}{(u-v)^2} + \frac{e^{-(u+v)/2}}{(u+v)^2}\right\} - \frac{4}{(u^2-v^2)^2}. \tag{58}$$

For $v > 0$ one can use, especially for $u \to v$, the equivalent forms

$$\bar{T}_1(u,v) = \frac{1}{u}\left\{\frac{e^{-(u-v)/2}-1}{u-v} + \frac{e^{-(u+v)/2}}{u+v}\right\} - \frac{1}{u(u+v)}, \tag{59}$$

$$\bar{T}_2(u,v) = \frac{1}{u^2}\left\{\left[\frac{u+2}{2u}\right]\left[\frac{e^{-(u-v)/2}}{u-v} + \frac{e^{-(u+v)/2}}{u+v}\right]\right.$$

$$\left. + \frac{e^{-(u-v)/2}-1}{(u-v)^2} + \frac{e^{-(u+v)/2}}{(u+v)^2}\right\} - \frac{3u+v}{u^2(u+v)(u^2-v^2)}. \tag{60}$$